

Engineered Upconversion Nanoparticles for Resolving Protein Interactions inside Living Cells

Christoph Drees, Athira Naduviledathu Raj, Rainer Kurre, Karin B. Busch, Markus Haase,* and Jacob Piehler*

Abstract: Upconversion nanoparticles (UCNPs) convert near-infrared into visible light at much lower excitation densities than those used in classic two-photon absorption microscopy. Here, we engineered <50 nm UCNPs for application as efficient lanthanide resonance energy transfer (LRET) donors inside living cells. By optimizing the dopant concentrations and the core-shell structure for higher excitation densities, we observed enhanced UCNP emission as well as strongly increased sensitized acceptor fluorescence. For the application of these UCNPs in complex biological environments, we developed a biocompatible surface coating functionalized with a nanobody recognizing green fluorescent protein (GFP). Thus, rapid and specific targeting to GFP-tagged fusion proteins in the mitochondrial outer membrane and detection of protein interactions by LRET in living cells was achieved.

Lanthanide-doped upconversion nanoparticles (UCNPs) convert two or more near-infrared (NIR) photons into one UV/Vis photon.^[1] Owing to the long-lived metastable energy levels of the lanthanide ions, NIR photons can be absorbed sequentially in upconversion materials. At low to moderate excitation densities, photon upconversion therefore shows much higher efficiency than other nonlinear optical processes such as two-photon excitation fluorescence.^[1b,n,2] Consequently, UCNPs can be excited with negligible luminescent background, yielding promising features for bioimaging and biosensing.^[1a,3]

A severe limitation of UCNPs is that their quantum yield is much lower than that compared to the bulk material; this is attributed to energy losses at crystal defects and energy migration to the surface of the nanoparticles.^[4] Moreover, the low concentrations of the optically active erbium or thulium ions (e.g. $[\text{Er}^{3+}] = 2\%$) traditionally employed to avoid energy losses by cross-relaxation result in low absorption cross sections of the particles.^[1b] There have been several approaches to cope with these challenges including the use of host materials with low phonon energy,^[1b] crystal modifications, various shell concepts,^[5] and surface plasmon coupling.^[6] In the work presented here we have used much higher dopant concentrations than traditionally used for bulk upconversion phosphors, since high doping levels have been reported to greatly increase the upconversion intensity of UCNPs at higher excitation densities.^[7]

Exciting possibilities arise from lanthanide resonance energy transfer (LRET) from UCNPs to acceptors like fluorescent dyes,^[8] photodynamic reagents,^[9] and gold nanoparticles.^[10] Compared to traditional Förster resonance energy transfer (FRET), upconversion LRET ensures highly specific detection of sensitized fluorescence of the acceptor,^[11] which typically is not directly excited under conditions of UCNP excitation. Accordingly, there have been numerous reports on UCNP-based LRET biosensors for detecting various molecular species.^[11,12] A majority of these sensors, however, probe LRET-dependent quenching of UCNPs,^[11] which lacks robustness when applied in live cell microscopy: owing to their low quantum yield, core-only UCNPs are rather dim probes. As quenching is accompanied by loss of emission intensity, proper detection and quantification are hindered. By contrast, the enhanced and commonly used core-shell UCNPs provide much higher emission intensity, but at the expense of low energy transfer efficiency. Therefore, a critical shell thickness for best LRET performance exists,^[13] and typically a relative high number of acceptor dyes per UCNP is required for efficient quenching, which is not desirable for cellular applications.



Application of UCNPs as cellular sensors and actuators in living cells introduces further challenges to nanoparticle design,^[14] which are particularly demanding when targeting proteins in the cytoplasm. For a minimum bias and thus functionality of conjugated proteins in the cytoplasm, nanoparticles must be kept small (hydrodynamic diameter <50 nm).^[15] To overcome nonspecific binding to cellular components and recognition by metabolic machineries within the cell,^[16] appropriate surface passivation is required that interferes with non-specific protein interactions yet maintains colloidal stability. Furthermore, site-specific conjugation with

[*] C. Drees, Prof. Dr. J. Piehler
Abteilung für Biophysik
Fachbereich Biologie/Chemie, Universität Osnabrück
Barbarastrasse 11, 49076 Osnabrück (Germany)
E-mail: piehler@uos.de

A. N. Raj, Prof. Dr. M. Haase
Institut für Chemie Neuer Materialien
Fachbereich Biologie/Chemie, Universität Osnabrück
Barbarastrasse 7, 49069 Osnabrück (Germany)
E-mail: markus.haase@uni-osnabrueck.de

Dr. R. Kurre
Center for Advanced Light Microscopy
Fachbereich Biologie/Chemie, Universität Osnabrück
Barbarastrasse 11, 49076 Osnabrück (Germany)

Prof. Dr. K. B. Busch
Fachbereich Biologie, Universität Münster
Schlossplatz 5, 48149 Münster (Germany)

 Supporting information and the ORCID identification number(s) for the author(s) of this article can be found under:
 <http://dx.doi.org/10.1002/anie.201603028>.

target proteins in the complex cellular environments requires bio-orthogonal functionalization strategies. To date, there are only few examples of live cell targeting of UCNP, exploiting antibody–antigen^[17] and receptor–ligand^[18] interactions. However, upconversion LRET from specifically targeted UCNP to acceptor fluorophores in living cells has not yet been reported.

We have here addressed these challenges by engineering UCNP as nanoscopic reporters for protein–protein interaction analysis inside living cells as depicted in Figure 1a. To

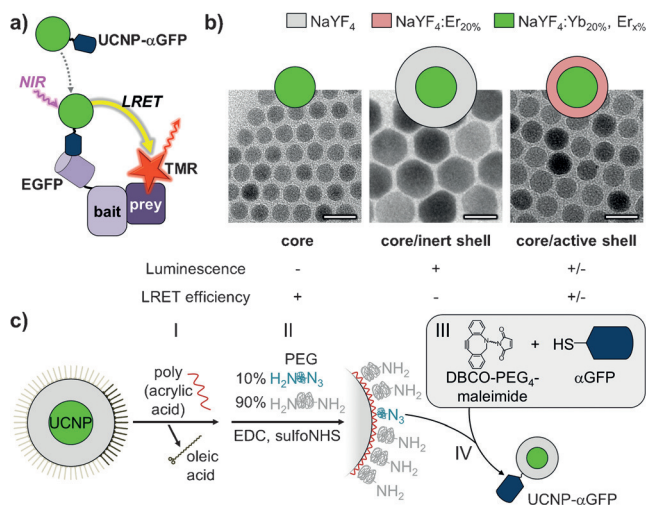


Figure 1. Concepts and strategies for designing an LRET reporter system. (a) UCNP functionalized with an anti-GFP nanobody (α GFP) are site-specifically targeted to a bait protein fused to EGFP. Interaction with an acceptor-tagged prey protein is detected by sensitized fluorescence upon LRET from the UCNP. (b) Different architectures and predicted properties of UCNP used in this study. Cartoons and transmission electron micrographs. Scale bars: 20 nm. (c) Biofunctionalization of UCNP including solubilization with poly(acrylic acid) (PAA) (I), PEGylation with a mixture of homo- and heterobifunctional poly(ethylene glycols) (PEGs) (II), and conjugation with nanobodies via site-specifically conjugated dibenzocyclooctyne (DBCO; III) for a copper-free click reaction with surface azides (IV).

ensure minimum bias of protein function within the cell, we focused on UCNP diameters below 30 nm, that is, dimensions similar to those of larger proteins complexes, which we aim to probe by LRET. To better exploit the photophysical properties of UCNP, we implemented a microscope for live-cell imaging providing continuous-wave laser excitation at 978 nm up to power densities of 20 kW cm⁻² (Figure S1a). In contrast to conventional picosecond or femtosecond excitation with a Ti:sapphire laser, other nonlinear optical phenomena such as two-photon fluorescence are not evoked under these conditions (Figure S1b), thus ensuring selective acceptor excitation via LRET. For compatibility with live-cell imaging, samples were mounted in an incubation chamber (Figure S1a) and immersed in aqueous buffer solution. Heating of the sample due to water absorption at 980 nm was avoided by relatively short illumination times (50 ms).

To achieve balanced levels of upconversion emission and LRET efficiency at these high excitation power densities, we

revisited UCNP design strategies with respect to core–shell architectures and doping densities. First, we systematically investigated the impact of an inert shell, the Er³⁺ concentration within the UCNP core, and the architecture of the active shell (Figure 1b). Monodisperse, hexagonal UCNP (Figure S2–S5) were synthesized as described previously^[19] and rendered water-soluble by exchanging the oleic acid ligands on the UCNP surface for poly(acrylic acid) (PAA) (Figure 1c). PAA-coated UCNP were subsequently PEGylated, which has been shown to minimize recognition by intracellular degradation machineries.^[16] PEGylated UCNP were site-specifically conjugated with a recombinant nanobody against GFP via a short crosslinker using click chemistry to ensure close proximity (Figure 1c). This roughly 10 kDa protein derived from llama heavy-chain antibodies very rapidly binds GFP fusion proteins with sub-nanomolar affinity.^[20]

For screening the photophysical properties of UCNP with respect to brightness and energy transfer efficiency, we developed a surface-based *in vitro* assay to probe LRET under physiological conditions. Negatively charged PAA-coated UCNP were immobilized onto a glass support functionalized with positively charged polyethylenimine (PEI). PEI was functionalized with tetramethylrhodamine (TMR), which served as an LRET acceptor for the green emission of the UCNP ($^2\text{H}_{11/2} \rightarrow ^4\text{I}_{15/2}$; $^4\text{S}_{3/2} \rightarrow ^4\text{I}_{15/2}$; Figure S6). TMR emission upon excitation at 978 nm can be exclusively ascribed to LRET (Figure S7), because two-photon excitation does not occur at these power densities. As a starting point, we chose a common core/inert-shell design ($\beta\text{-NaYF}_4\text{:Yb}_{20\%}\text{Er}_{2\%}/\beta\text{-NaYF}_4$, $d_{\text{core}} = 11$ nm; $r_{\text{shell}} = 7$ nm), which had been reported to be two or three orders of magnitude brighter than the corresponding core UCNP.^[4a] When the excitation power was increased from 1 to 18 kW cm⁻², a substantial increase of UCNP emission (ca. 17 \times) and LRET (ca. 37 \times) was observed (Figure 2a). At power densities above 2.5 kW cm⁻², however, the slope of the curve substantially decreased. In contrast, a linear increase of both UCNP emission and LRET up to an excitation power density of 18 kW cm⁻² was observed for core-only UCNP (Figure 2a). Under these conditions, the level of sensitized acceptor fluorescence was similar to that of core–shell particles, while the UCNP emission intensity was roughly one-fifth, confirming a higher LRET efficiency probably caused by closer proximities of the acceptor in the absence of a shell. Importantly, even at the highest excitation power densities, no significant heating within the incubation chamber was observed.

To explore the influence of cross relaxation, core/shell nanoparticles doped with different Er³⁺ concentrations ranging from 2% up to 20% were analyzed (Figure 2b). In contrast to the power-dependent saturation observed for UCNP emission and LRET of 2% Er³⁺ UCNP, higher dopant concentrations led to much higher, close to linear increase of UCNP and LRET. Thus, for the 5% Er³⁺ UCNP the emission intensity was five times higher and the LRET intensity was three times higher than the analogous intensities for 2% Er³⁺ UCNP. A similar enhancement of the UCNP emission and LRET was observed for particles containing

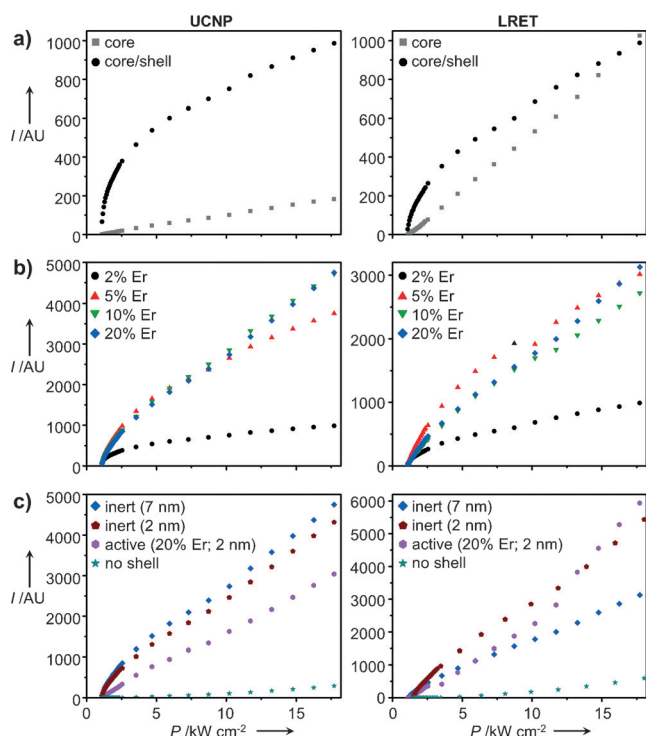


Figure 2. Power dependence of UCNP emission (left) and LRET (right) of various UCNPs. (a) Comparison of core and core/inert shell. (b) Comparison of Er³⁺ concentrations in the core of core/inert shell UCNPs. (c) Shell designs. 20% Er³⁺ in the core. If not mentioned otherwise: core: $\beta\text{-NaYF}_4\text{:Yb}_{20\%}\text{Er}_{20\%}$ ($d \approx 11$ nm), inert shell: $\beta\text{-NaYF}_4$ ($r \approx 7$ nm). Data was extracted from microscopy experiments with a 978 nm continuous-wave laser and filters for the green emission band of UCNPs (500–570 nm) and LRET (593–604 nm). Due to experimental settings, absolute signals of UCNPs and LRET channels are not comparable.

10% and 20% Er³⁺. Because the optical properties of UCNPs benefited from elevated Er³⁺ concentrations, we investigated the combination of 20% Er³⁺ UCNPs with a thin shell (2 nm) consisting either of inert $\beta\text{-NaYF}_4$ or doped $\beta\text{-NaYF}_4\text{:Er}_{20\%}$ (cf. Figure 1b).

We speculated that upconversion would occur between Yb³⁺ and Er³⁺ in the core and that in the latter case the energy would be able to migrate to the surface via Er³⁺ ions in the shell. Indeed, UCNPs with a thin inert shell exhibited emission intensities comparable to those of nanoparticles with a thick shell, but twofold enhanced LRET (Figure 2c). The emission of the UCNPs with Er³⁺-doped shell was about 30% weaker than emission of inert-shell UCNPs, presumably due to surface quenching. Strikingly, the LRET power dependence of active-shell UCNPs was nonlinear (exponent ≈ 1.6), reaching a level comparable to that of inert-shell UCNPs at 18 kW cm⁻² (Figure 2c). Emission and LRET of non-shell $\beta\text{-NaYF}_4\text{:Yb}_{20\%}\text{Er}_{20\%}$ UCNPs were significantly decreased compared to all other systems, indicating strong energy migration to the surface and quenching on the surface (Figure 2c). Taken together, the combination of elevated excitation power density and thin-shell $\beta\text{-NaYF}_4\text{:Yb}_{20\%}\text{Er}_{20\%}/\beta\text{-NaYF}_4$ nanoparticles enhanced UCNP emission and LRET by more than two orders of

magnitude compared to standard $\beta\text{-NaYF}_4\text{:Yb}_{20\%}\text{Er}_{20\%}/\beta\text{-NaYF}_4$ core/shell particles at low power density.

With these improved probes at hand, we generated biocompatible UCNPs conjugated with anti-GFP nanobodies (UCNP- αGFP , < 50 nm, cf. Figure 1c) and explored their targeting to GFP fusion proteins inside living cells. For this purpose, biofunctionalized UCNPs were microinjected into HeLa cells stably expressing Tom20 fused to monomeric EGFP and the HaloTag^[21] (Tom20-EGFP-HaloTag). Tom20 is a subunit of the heterooligomeric translocase of the outer mitochondrial membrane (TOM) complex^[22] and served as marker for the mitochondrial network, which, because of its characteristic shape, is a robust readout for targeting quality. By optional labeling of the HaloTag with TMR conjugated to the HaloTag ligand, Tom20-EGFP-HaloTag was suitable for testing upconversion LRET to TMR as acceptor (Figure 3a).

Shortly after microinjection, UCNPs- αGFP quantitatively colocalized with the characteristic mitochondrial network visualized by EGFP fluorescence of Tom20-EGFP-HaloTag (Figure 3b). The specificity of UCNPs targeting was confirmed by several controls. In the absence of UCNPs, no signal was

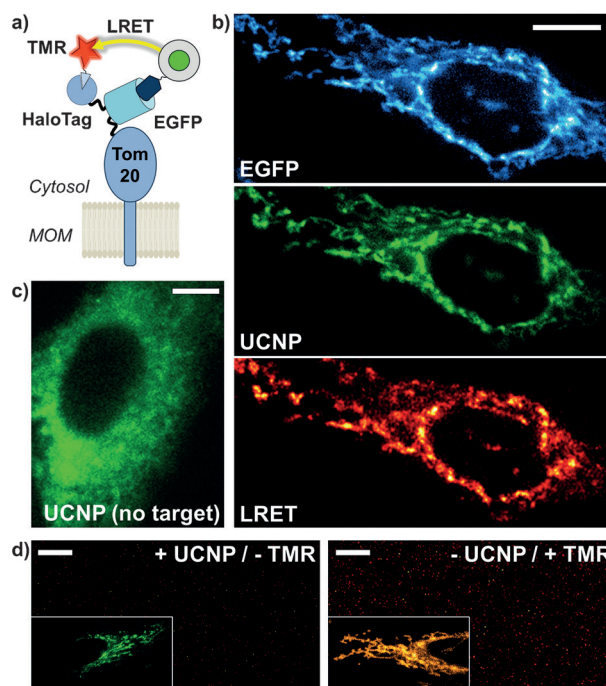


Figure 3. Selective targeting of UCNPs- αGFP as the reporter in living cells. (a) Cartoon of the assay: the fusion protein Tom20-EGFP-HaloTag localized in the mitochondrial outer membrane (MOM) ensures UCNPs- αGFP targeting via EGFP and an optional LRET acceptor by labeling with TMR via the HaloTag. (b) Selective binding of UCNPs- αGFP injected into HeLa cells stably expressing Tom20-EGFP-HaloTag, which was labeled with TMR. Top: EGFP fluorescence upon excitation at 488 nm; middle: UCNP emission (500–570 nm) upon excitation at 978 nm; bottom: sensitized TMR emission (593–607 nm) upon excitation at 978 nm. (c) UCNPs- αGFP injected into a HeLa cell, which did not express any GFP fusion protein. (d) No sensitized TMR emission (593–607 nm) upon excitation at 978 nm in the absence of TMR (left) or UCNPs (right). Insets: UCNP emission upon excitation at 978 nm (left) and TMR emission upon excitation at 520–550 nm (right). Scale bars: 10 μm .

detectable upon excitation at 978 nm (Figure S8). Upon injection into HeLa cells lacking a GFP-tagged target protein, UCNP- α GFP was homogeneously distributed. These observations confirmed free diffusion of functionalized UCNPs within the cell and highly specific subcellular targeting (Figure 3c). The extended mitochondrial network, which is highly sensitive to stress including potential local heating caused by UCNP excitation, was maintained during targeting and imaging of UCNPs. These results indicated full cell viability and minimum bias of organellar function caused by the engineered UCNPs and by their excitation at high power densities. By comparison with the UCNP monolayer experiments performed in vitro, a typical density of 1–10 particles per μm^2 bound at the MOM was estimated. Strikingly, upconversion LRET to TMR-labeled Tom20-EGFP-HaloTag was detectable after UCNP- α GFP targeting (Figure 3b). By contrast, the absence of either UCNPs or TMR resulted in no signal above detector noise in the TMR channel, highlighting the selectivity of UCNP LRET (Figure 3d). Conventional FRET experiments carried out for the same system but in the absence of UCNPs highlighted the unique selectivity of LRET with respect to acceptor emission (Figure S9).

As a proof-of-concept application of UCNP LRET as a nanoscopic reporter for protein–protein interactions in living cells we investigated the interaction of Tom20 with Tom7, which is another subunit of the TOM complex. Since the two proteins do not interact directly with each other, but are associated with and spatially separated by Tom40^[23] (Figure 4a), the distance between Tom20 and Tom7 is too

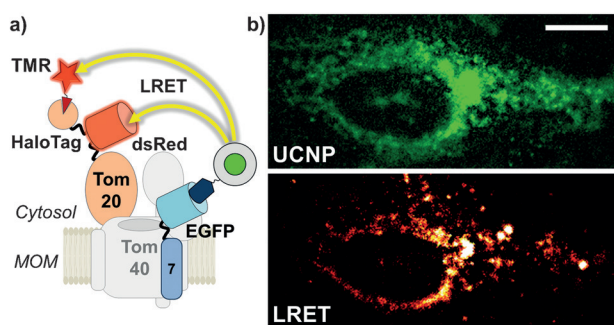


Figure 4. Detection of distal interaction partners. (a) UCNP- α GFP were attached to EGFP-Tom7 in the mitochondrial outer membrane (MOM), which was coexpressed with Tom20 fused to the LRET acceptors dsRed and HaloTag labeled by TMR. (b) Visualization of the indirect Tom7–Tom20 interaction by LRET. Top: UCNP emission (500–570 nm) upon excitation at 978 nm; bottom: sensitized TMR emission (593–607 nm) upon excitation at 978 nm. Scale bar: 10 μm .

large for unambiguous detection with conventional FRET probes. We co-expressed Tom7 fused to monomeric EGFP with Tom20-dsRed-HaloTag in HeLa cells and labeled with UCNP- α GFP and TMR, respectively (Figure 4a). Specific targeting of UCNP- α GFP to EGFP-Tom7 was confirmed by colocalization with the mitochondrial network (Figure S10). Strikingly, LRET-sensitized TMR emission could be detected in this assay (Figure 4b), demonstrating that the system is capable of reporting indirect, long-distance interactions.

Monitoring and manipulating protein interactions inside living cells without affecting biological functions stands as a current major challenge in molecular cell biology.^[24] Nanoparticle-based approaches have high potential in this field, but massive efforts are still required in order to tailor physico-chemical and biological properties to achieve unbiased interrogation in the cellular context. Here, we have successfully engineered UCNPs as LRET reporter probes for protein interactions in the cytoplasm of live cells. This achievement was possible by exploiting the unique photophysical properties of UCNPs at elevated excitation power density. Through increased doping levels and an optimized shell thickness, we could increase sensitized acceptor fluorescence by two orders of magnitude. Thus, UCNPs with diameters below 30 nm could be employed, ensuring unhindered mobility in the cytosol and reduced bias due to protein crosslinking. Ultra-thin, highly biocompatible surface coating in combination with rapid and efficient targeting via an anti-GFP nanobody allows for versatile application of these UCNPs as nanoscopic reporters of protein interactions in living cells. We experimentally confirmed well controlled, precise targeting of UCNPs in the cytoplasm while fully maintaining cell viability. Thus, we succeeded in detecting direct and indirect protein–protein interactions by upconversion LRET in living cells. In contrast to conventional FRET reporters, detection of sensitized acceptor fluorescence in an upconversion LRET format yielded negligible background. Thus, in situ proximity analysis can be achieved with high fidelity, which has tremendous potential for unraveling the spatiotemporal organization of protein complexes in cells. These proof-of-concept experiments establish exciting opportunities for novel bioanalytical applications of UCNPs, for example, for noninvasive nanoscopic photochemical manipulation by upconversion LRET. Substantial further UCNP optimization along the lines we have highlighted in this work will be possible, allowing for the application of much smaller UCNPs. Thus, even less bias of protein function and more facile delivery into the cytosol can be achieved, as well as further increased spatial resolution.

Acknowledgements

We thank Gabriele Hikade, Hella Kenneweg, Junel Sotolongo Bellon, and Wladislaw Kohl for technical support as well as Domenik Liße, Christian Richter, Jörg Nordmann, Thorben Rinkel, and Changjiang You for helpful advice. This project was supported by the Deutsche Forschungsgemeinschaft (SFB 944) and by the European Commission (FET-open 686841—MAGNEURON).

Keywords: biosensors · LRET · nanoparticles · TOM complexes · upconversion

How to cite: *Angew. Chem. Int. Ed.* **2016**, *55*, 11668–11672
Angew. Chem. **2016**, *128*, 11840–11845

- [1] a) F. Wang, D. Banerjee, Y. Liu, X. Chen, X. Liu, *Analyst* **2010**, *135*, 1839–1854; b) M. Haase, H. Schafer, *Angew. Chem. Int. Ed.* **2011**, *50*, 5808–5829; *Angew. Chem.* **2011**, *123*, 5928–5950; c) X.

- Liu, C. H. Yan, J. A. Capobianco, *Chem. Soc. Rev.* **2015**, *44*, 1299–1301; d) F. Auzel, *Chem. Rev.* **2004**, *104*, 139–173; e) B. Zhou, B. Shi, D. Jin, X. Liu, *Nat. Nanotechnol.* **2015**, *10*, 924–936; f) H. H. Gorris, O. S. Wolfbeis, *Angew. Chem. Int. Ed.* **2013**, *52*, 3584–3600; *Angew. Chem.* **2013**, *125*, 3668–3686; g) F. Wang, X. Liu, *Chem. Soc. Rev.* **2009**, *38*, 976–989; h) D. K. Chatterjee, M. K. Gnanasamandhan, Y. Zhang, *Small* **2010**, *6*, 2781–2795; i) D. Vennerberg, Z. Lin, *Sci. Adv. Mater.* **2011**, *3*, 26–40; j) J. F. Suyver, A. Aebischer, D. Biner, P. Gerner, J. Grimm, S. Heer, K. W. Krämer, C. Reinhard, H. U. Güdel, *Opt. Mater.* **2005**, *27*, 1111–1130; k) B. M. van der Ende, L. Aarts, A. Meijerink, *Phys. Chem. Chem. Phys.* **2009**, *11*, 11081–11095; l) A. Gnach, A. Bednarkiewicz, *Nano Today* **2012**, *7*, 532–563; m) C. T. Xu, Q. Zhan, H. Liu, G. Somesfalean, J. Qian, S. He, S. Andersson-Engels, *Laser Photonics Rev.* **2013**, *7*, 663–697; n) G. Chen, H. Agren, T. Y. Ohulchanskyy, P. N. Prasad, *Chem. Soc. Rev.* **2015**, *44*, 1680–1713.
- [2] a) D. R. Gamelin, H. U. Güdel, *Acc. Chem. Res.* **2000**, *33*, 235–242; b) F. E. Auzel, *Proc. IEEE* **1973**, *61*, 758–786.
- [3] H. S. Mader, P. Kele, S. M. Saleh, O. S. Wolfbeis, *Curr. Opin. Chem. Biol.* **2010**, *14*, 582–596.
- [4] a) F. Wang, J. Wang, X. Liu, *Angew. Chem. Int. Ed.* **2010**, *49*, 7456–7460; *Angew. Chem.* **2010**, *122*, 7618–7622; b) J.-C. Boyer, F. C. J. M. van Veggel, *Nanoscale* **2010**, *2*, 1417–1419.
- [5] a) F. Zhang, R. Che, X. Li, C. Yao, J. Yang, D. Shen, P. Hu, W. Li, D. Zhao, *Nano Lett.* **2012**, *12*, 2852–2858; b) X. Liu, X. Kong, Y. Zhang, L. Tu, Y. Wang, Q. Zeng, C. Li, Z. Shi, H. Zhang, *Chem. Commun.* **2011**, *47*, 11957–11959; c) H.-X. Mai, Y.-W. Zhang, L.-D. Sun, C.-H. Yan, *J. Phys. Chem. C* **2007**, *111*, 13721–13729; d) Y. Wang, L. Tu, J. Zhao, Y. Sun, X. Kong, H. Zhang, *J. Phys. Chem. C* **2009**, *113*, 7164–7169; e) N. J. J. Johnson, A. Korinek, C. Dong, F. C. J. M. van Veggel, *J. Am. Chem. Soc.* **2012**, *134*, 11068–11071; f) F. Vetrone, R. Naccache, V. Mahalingam, C. G. Morgan, J. A. Capobianco, *Adv. Funct. Mater.* **2009**, *19*, 2924–2929; g) D. Yang, C. Li, G. Li, M. Shang, X. Kang, J. Lin, *J. Mater. Chem.* **2011**, *21*, 5923–5927; h) B. Voss, M. Haase, *ACS Nano* **2013**, *7*, 11242–11254; i) S. Dühnen, M. Haase, *Chem. Mater.* **2015**, *27*, 8375–8386; j) T. Rinkel, A. N. Raj, S. Dühnen, M. Haase, *Angew. Chem. Int. Ed.* **2016**, *55*, 1164–1167; *Angew. Chem.* **2016**, *128*, 1177–1181.
- [6] a) S. Han, R. Deng, X. Xie, X. Liu, *Angew. Chem. Int. Ed.* **2014**, *53*, 11702–11715; *Angew. Chem.* **2014**, *126*, 11892–11906; b) S. Schietinger, T. Aichele, H. Q. Wang, T. Nann, O. Benson, *Nano Lett.* **2010**, *10*, 134–138; c) H. Zhang, Y. Li, I. A. Ivanov, Y. Qu, Y. Huang, X. Duan, *Angew. Chem. Int. Ed.* **2010**, *49*, 2865–2868; *Angew. Chem.* **2010**, *122*, 2927–2930; d) M. Fujii, T. Nakano, K. Imakita, S. Hayashi, *J. Phys. Chem. C* **2013**, *117*, 1113–1120; e) W. Feng, L.-D. Sun, C.-H. Yan, *Chem. Commun.* **2009**, 4393–4395; f) P. Yuan, Y. H. Lee, M. K. Gnanasamandhan, Z. Guan, Y. Zhang, Q.-H. Xu, *Nanoscale* **2012**, *4*, 5132–5137; g) F. Zhang, G. B. Braun, Y. Shi, Y. Zhang, X. Sun, N. O. Reich, D. Zhao, G. Stucky, *J. Am. Chem. Soc.* **2010**, *132*, 2850–2851.
- [7] a) D. J. Gargas, E. M. Chan, A. D. Ostrowski, S. Aloni, M. V. Altoe, E. S. Barnard, B. Sani, J. J. Urban, D. J. Milliron, B. E. Cohen, P. J. Schuck, *Nat. Nanotechnol.* **2014**, *9*, 300–305; b) J. Zhao, D. Jin, E. P. Scharfner, Y. Lu, Y. Liu, A. V. Zvyagin, L. Zhang, J. M. Dawes, P. Xi, J. A. Piper, E. M. Goldys, T. M. Monro, *Nat. Nanotechnol.* **2013**, *8*, 729–734.
- [8] Y. X. Wu, X. B. Zhang, D. L. Zhang, C. C. Zhang, J. B. Li, Y. Wu, Z. L. Song, R. Q. Yu, W. Tan, *Anal. Chem.* **2016**, *88*, 1639–1646.
- [9] a) X. Wang, K. Liu, G. Yang, L. Cheng, L. He, Y. Liu, Y. Li, L. Guo, Z. Liu, *Nanoscale* **2014**, *6*, 9198–9205; b) Z. Zhao, Y. Han, C. Lin, D. Hu, F. Wang, X. Chen, Z. Chen, N. Zheng, *Chem. Asian J.* **2012**, *7*, 830–837; c) D. K. Chatterjee, L. S. Fong, Y. Zhang, *Adv. Drug Delivery Rev.* **2008**, *60*, 1627–1637.
- [10] a) H. Chen, F. Yuan, S. Wang, J. Xu, Y. Zhang, L. Wang, *Biosens. Bioelectron.* **2013**, *48*, 19–25; b) L. Wang, R. Yan, Z. Huo, L. Wang, J. Zeng, J. Bao, X. Wang, Q. Peng, Y. Li, *Angew. Chem. Int. Ed.* **2005**, *44*, 6054–6057; *Angew. Chem.* **2005**, *117*, 6208–6211.
- [11] W. Zheng, P. Huang, D. Tu, E. Ma, H. Zhu, X. Chen, *Chem. Soc. Rev.* **2015**, *44*, 1379–1415.
- [12] a) W. W. Ye, M. K. Tsang, X. Liu, M. Yang, J. Hao, *Small* **2014**, *10*, 2390–2397; b) S. Zhang, J. Wang, W. Xu, B. T. Chen, W. Yu, L. Xu, H. W. Song, *J. Lumin.* **2014**, *147*, 278–283; c) M. Wang, W. Hou, C.-C. Mi, W.-X. Wang, Z.-R. Xu, H.-H. Teng, C.-B. Mao, S.-K. Xu, *Anal. Chem.* **2009**, *81*, 8783–8789; d) M. K. Tsang, W. Ye, G. Wang, J. Li, M. Yang, J. Hao, *ACS Nano* **2016**, *10*, 598–605.
- [13] Y. Wang, K. Liu, X. M. Liu, K. Dohnalova, T. Gregorkiewicz, X. G. Kong, M. C. G. Aalders, W. J. Buma, H. Zhang, *J. Phys. Chem. Lett.* **2011**, *2*, 2083–2088.
- [14] A. Sedlmeier, H. H. Gorris, *Chem. Soc. Rev.* **2015**, *44*, 1526–1560.
- [15] F. Etoc, C. Vicario, D. Lisse, J. M. Siaugue, J. Piehler, M. Coppey, M. Dahan, *Nano Lett.* **2015**, *15*, 3487–3494.
- [16] D. Lisse, C. P. Richter, C. Drees, O. Birkholz, C. You, E. Rampazzo, J. Piehler, *Nano Lett.* **2014**, *14*, 2189–2195.
- [17] M. Wang, C.-C. Mi, W.-X. Wang, C.-H. Liu, Y.-F. Wu, Z.-R. Xu, C.-B. Mao, S.-K. Xu, *ACS Nano* **2009**, *3*, 1580–1586.
- [18] a) K. Y. Lee, E. Seow, Y. Zhang, Y. C. Lim, *Biomaterials* **2013**, *34*, 4860–4871; b) C. Yao, C. Wei, Z. Huang, Y. Lu, A. M. El-Toni, D. Ju, X. Zhang, W. Wang, F. Zhang, *ACS Appl. Mater. Interfaces* **2016**, *8*, 6935–6943; c) L. L. Li, R. Zhang, L. Yin, K. Zheng, W. Qin, P. R. Selvin, Y. Lu, *Angew. Chem. Int. Ed.* **2012**, *51*, 6121–6125; *Angew. Chem.* **2012**, *124*, 6225–6229.
- [19] a) Y. Wei, F. Lu, X. Zhang, D. Chen, *Chem. Mater.* **2006**, *18*, 5733–5737; b) J. Nordmann, B. Voß, R. Komban, K. Kömpe, A. N. Raj, T. Rinkel, S. Dühnen, M. Haase, *Z. Phys. Chem.* **2015**, *229*, 247.
- [20] A. Kirchhofer, J. Helma, K. Schmidthals, C. Frauer, S. Cui, A. Karcher, M. Pellis, S. Muyldermans, C. S. Casas-Delucchi, M. C. Cardoso, H. Leonhardt, K. P. Hopfner, U. Rothbauer, *Nat. Struct. Mol. Biol.* **2010**, *17*, 133–138.
- [21] G. V. Los, L. P. Encell, M. G. McDougall, D. D. Hartzell, N. Karassina, C. Zimprich, M. G. Wood, R. Learish, R. F. Ohana, M. Urh, D. Simpson, J. Mendez, K. Zimmerman, P. Otto, G. Vidugiris, J. Zhu, A. Darzins, D. H. Klaubert, R. F. Bulleit, K. V. Wood, *ACS Chem. Biol.* **2008**, *3*, 373–382.
- [22] J. Dudek, P. Rehling, M. van der Laan, *Biochim. Biophys. Acta Mol. Cell Res.* **2013**, *1833*, 274–285.
- [23] T. Shiota, K. Imai, J. Qiu, V. L. Hewitt, K. Tan, H.-H. Shen, N. Sakiyama, Y. Fukasawa, S. Hayat, M. Kamiya, A. Elofsson, K. Tomii, P. Horton, N. Wiedemann, N. Pfanner, T. Lithgow, T. Endo, *Science* **2015**, *349*, 1544–1548.
- [24] J. Piehler, *Curr. Opin. Struct. Biol.* **2014**, *24*, 54–62.

Received: March 28, 2016

Revised: June 29, 2016

Published online: August 11, 2016